Journal of Ecology of Health & Environment
An International Journal

http://dx.doi.org/10.18576/jehe/130301

Turbulence Parameterization for Estimating Air Pollutant Concentration

Khaled S. M. Essa[1,], Ahmed M. Mosallem[1] and Fawzia Mubarak[2].*

[1] Egyptian Atomic Energy Authority, (EAEA), Nuclear Research Center (NRC), Mathematics and Theoretical Physics Department. Cairo, Egypt
[2] Egyptian Atomic Energy Authority (EAEA), Nuclear and Radiological Safety Research Center (NRSRC), Nuclear Fuel Cycle Safety Department, Cairo, Egypt

Received: 25 May. 2025, Revised: 15 Jul. 2025, Accepted: 20. Aug. 2025.
Published online: 1 Sep. 2025

Abstract: The distribution of pollutant mass is affected by turbulent diffusion, which presents significant issues. Wind shear, buoyancy, surface roughness, wind intensity, cloud cover, and velocity variations are all included in this topic. The particle-displacement probability distribution form, mean concentration field of continuous sources, apparent eddy diffusivity, initial phase of continuous plumes, atmospheric cloud growth far from concentrated sources, Lagrangian properties of turbulence, consequences of Taylor's theorem, elementary statistical theory of turbulent diffusion, and the Hay-Pasquill method for cloud-spread prediction were all discussed in order to characterize turbulent diffusion. The crosswind-integrated normalized concentration was predicted using the Gaussian plume model at the center-line at ground level and at vertical height using the evaluated turbulence coefficients. This was then compared with the three-dimensional Iodine-135 concentrations that were observed. The expected concentration and the observed concentration are in good agreement, according to a statistical analysis of the data.

Keywords: Turbulent diffusion; Hay-Pasquill approach; Eddy diffusivity; Taylor’s theorem.

1. Introduction

The distribution of pollutant mass and the complexity of atmospheric dispersion are both impacted by the behavior of discharged pollutants, which is determined by buoyancy and turbulence [1-3]. Turbulence is a flow phase characterized by chaotic, stochastic property changes and is a complicated structural phenomenon. Turbulence controls the great bulk of atmospheric dispersion. Turbulence is one of the most profound unsolved mysteries in classical physics, despite its ubiquitous presence [4]. Turbulent flows are the most important component for developing models to enhance comprehension for analysis and application [5-7]. The flow regime characterized by chaotic, stochastic changes in wind shear, buoyancy, surface roughness, wind intensity, cloud cover, velocity fluctuations, humidity, temperature, and rapid changes in pressure and flow velocity is known as turbulence, and it is a complex structural phenomenon [8-9],[2] and [10]. Understanding the causes of atmospheric turbulence is necessary to forecast the quantity of contaminants in the air. Turbulence intensity is considered to be the most significant element when assessing the pollutant concentrations at a recipient location in response to various fluxes [11-13]. Thermal agitation of molecules on a molecular size and turbulence on a macroscopic scale, where turbulent movement (i.e its larger intensity) is usually considerably greater than molecular, are two forms of random motions that commonly occur in air turbulence [14-15].

In this work we explain the distribution of pollutant mass is affected by turbulent diffusion. Also, we calculate the crosswind-integrated normalized concentration using the Gaussian plume model at the center-line at ground level and vertical height using the evaluated turbulence coefficients. This was then compared with the three-dimensional Iodine-135 concentrations that were observed. We find that the expected concentration and the observed concentration are in good agreement, according to a statistical analysis of the data.

2. Materials and Methods

An energy cascade is the term for this phenomenon, which can be described by appropriate experiments and statistical theory. The eddies of different sizes make up turbulent flow dissipate as heat [16]. One of the most important factors in establishing the internal structure of turbulence is the rate of total energy dissipation per unit mass (ε), which determines the parameters of turbulent flows. The selection of analysis techniques, averaging window, turbulence intensity, and large-scale random flow velocities can all have an impact on the estimation of the mean energy dissipation rate and its variations from the instantaneous energy dissipation rate. The dissipation rate ε determines the turbulent flow characteristics [17]. Turbulence seems to be composed of many "eddies," each of which has a distinct velocity scale um and length scale L. Numerous

*Corresponding author e-mail: mohamedksm56@yahoo.com

© 2025 NSP
Natural Sciences Publishing Cor.

quantitative factors can be used to describe the turbulence. One important aspect of air turbulence is the amplification of velocity fluctuations caused by abrupt changes in wind direction and speed. Eddies of varying sizes contribute to the turbulent energy in different ways because of their different velocities. For mass movement and disintegration, atmospheric eddies of all sizes are crucial [18]. Turbulent "intensity," or mean-square velocity in a given coordinate direction, $\overline{\acute{u}^2}$, $\overline{\acute{v}^2}$, and $\overline{\acute{w}^2}$ where ú, ṽ, and ẃ are the "turbulent" components of the velocity, is one of the most important features of turbulent flow [19] state that the mean fluctuating velocity's components (gustiness or relative intensity) are explained as follows if its magnitude is U:

$$i_x = \frac{\overline{(\acute{u}^2)}^{1/2}}{U}$$

$$i_y = \frac{\overline{(\acute{v}^2)}^{1/2}}{U}$$

$$i_z = \frac{\overline{(\acute{w}^2)}^{1/2}}{U} \quad (1)$$

$u_m = \left(\overline{\acute{u}^2}\right)^{1/2}$ is the square root of velocity. One can accurately describe the typical eddy, its characteristic size, or its scale L by taking a record of velocity variations u′ at point "A" and another record at the nearby location "B" at the same time. If the two points are very close to each other, the records are nearly the same; if they are very far apart, they have no connection at all. The mean square turbulent velocity, which makes up most of the turbulent energy, can be defined as the distance at which the relationship becomes negligible. A spectrum of turbulent energy over the eddy sizes can be derived by isolating eddies of a particular size and computing their average characteristic velocity, or the average kinetic energy per unit mass carried by them. Measurable factors and statistical concepts were examined in this work in order to define the turbulence for determining the concentration of air contaminants.

Basic turbulent diffusion statistics theory:

According to [20], modeling the concentration's probability distribution can adequately define the amplitude and likelihood of concentration fluctuations. It is evident from the fundamentals of turbulence that concentration changes will take place on the scale of the typical eddy size, L, resulting in a very erratic profile in terms of both time and space [21]. The concentration history at fixed x is a stationary process under various conditions following such a persistent source, but the observed (instantaneous) concentration fluctuates at random at any fixed-point x. The "elementary statistical theory" of turbulent diffusion states that the ensemble-mean concentration at a given time t is equal to the time-average concentration that is obtained by averaging the concentrations. This time-average concentration field at a fixed site can be associated with particle displacement probabilities.

Mathematical Modeling of Turbulent Diffusion

One of the most popular models for predicting pollutant dispersion is the Lagrangian Particle Dispersion Model (LPDM), which simulates the paths taken by individual pollution particles as they move through a turbulent flow. These models take into account the random nature of turbulence by use statistical techniques to represent the dispersion process [22]. Second, the Turbulent Kinetic Energy (TKE) Model uses the concept of turbulent kinetic energy to characterize the degree of turbulence and forecasts how pollutants will spread by evaluating the energy available for turbulent mixing [6]. The most important model is the Gaussian Plume Model, which is simple, practical, and has a high spatial resolution [23]. This model assumes that the concentration of pollutants spreads outward from the source in a Gaussian distribution, accounting for factors such as wind speed, air stability, and eddy diffusion coefficients [5].

Turbulence's Lagrangian Properties

[24] claim that the physics of dispersion is closely connected to the Lagrangian explanation of turbulence, which is simple. The random motions of a diffusing particle in such a field are made up of both the movements of continuum elements, or irregular bulk motion, and a superimposed Brownian motion, or molecular motion [25-26]. Since even the smallest turbulent eddy and the mean free route differ greatly in scale, the mean square displacements or velocities are essentially the total of squares coming from either source, and these two motions happen separately. The following is an expression for mean square displacements $\sigma_{xt}^2$when turbulent bulk motion only occurs along the x-axis:

$$\sigma_x^2 = \sigma_{xt}^2 + 2Dt \quad (2)$$

In most environmental applications, the molecular contribution 2Dt is negligible and $\sigma_x = \sigma_{xt}$. The real shape of the Lagrangian correlation function $R(\tau)$ for stationary and homogeneous turbulence has not yet been adequately predicted theoretically [27],[4]. With the exception of phenomena influenced by the shape of the autocorrelation function at small r, satisfying experimental agreement with theory is obtained assuming a Markov process. The exponential-decay autocorrelation function of a Markov process is:

$$R(\tau) = e^{-t/t_L} \quad (3)$$

where, the appropriate time scale is t_L. When Eq. (3) is used, the velocity history of a fluid element $t_L$is transformed into the "Lagrangian time scale". In Brownian motion, this is also a Markov process and may be written as $t_L = \beta^{-1}$. On the other hand, the Lagrangian time scale in turbulent flow is a characteristic of the energy-containing eddies and may be determined by computing $t_L = \text{const}\, L/u_m$, where the constant is of order unity, using the eddies' length scale L and velocity scale u_m. Because $R(\tau)$

© 2025 NSP
Natural Sciences Publishing Cor.

is an even function, the argument τ in Eq. (3) should more precisely represent the absolute value τ. Its expansion at $\tau = 0$ should be as follows, given the properties of $R(\tau)$ that are applicable to all stationary stochastic processes:

$$R(\tau) = 1 - \left(\frac{\tau}{t_m}\right)^2 + \cdots (\tau \to 0) \quad (4)$$

where tm is a Lagrangian microscale, which is the τ-axis intercept of the osculating parabola of $R(\tau)$ at $\tau = 0$ [28]. These characteristics of $R(\tau)$ are shown in Fig. (1) for the scenario in which a Markov process model is almost accurate. The following arguments and the mean square dispersion along the y-axis are valid if the velocity history of a diffusing particle is a stationary process [29];

$$\sigma_y^2 = 2\overline{v^2}\int_0^t (t-\tau)R(\tau)d\tau \quad (5)$$

The behavior of $R(\tau)$ at small and large values of the lag-time τ leads to several significant asymptotic features of σ_y. Since $R(\tau) \to 1$ and $\tau \to 0$, Eq. (5) produces:

$$\sigma_y^2 = \overline{v^2}t^2 - 0(t^4) \qquad (t \to 0) \quad (5a)$$

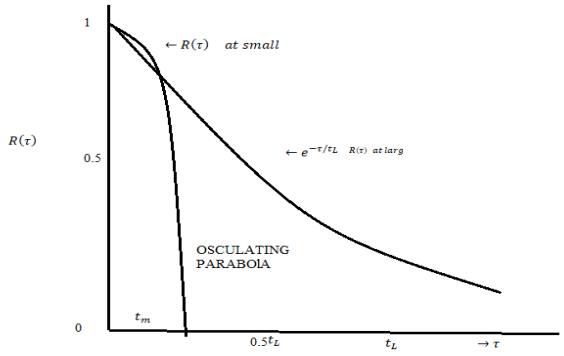

Fig. 1: shows the Lagrangian correlation function's characteristics.

Taylor's Theorem Consequences

In this case, it is assumed that σ_y first rises linearly with time (rather than with the square root of time as in Brownian or molecular diffusion). Conversely, if we suppose that the correlation tends to zero quickly enough for $\int_0^\infty \tau R(\tau)\, d\tau$ to exist, we discover that as $\tau \to \infty$, $R(\tau) \to 0$.

$$\sigma_y^2 = 2\overline{v^2}t_0(t - t_1) \quad (t \to \infty) \quad (5b)$$

where,

$$t_0 = \int_0^\infty R(\tau)\, d\tau$$

$$t_1 = \frac{1}{t_0}\int_0^\infty \tau R(\tau)\, d\tau \qquad (if \quad t_0 \neq 0)$$

where, if t_0 is not zero, $t_0$is the area under the $R(\tau)$ curve and t_1 is its center of gravity. When wave-like motions are present, the area under the $R(\tau)$ curve, or t_0, may reach zero. A correlation function of this kind is

$$R(\tau) = e^{-m\tau}\left(\cos n\tau - \frac{m}{n}\sin n\tau\right) \quad (6)$$

(Eq. (5) is not satisfied). The initial moment $\int_0^\infty \tau\, R(\tau)d\tau$ this kind is often unfavorable, and it was

$$\sigma_y^2 = 2\overline{v^2}t_2^2 = const. \qquad (t \to \infty) \quad (t_0 = 0) \quad (7)$$

With

$$t_2^2 = -\int_0^\infty \tau R(\tau)d\tau$$

Eq. (4) as $t_1 = t_0 = t_L$ for the exceptional case of a correlation functions of exponential decay type. By replacing β^{-1} with t_L in Taylor's theorem, the mean square dispersion can be found. Fig. (2) shows how σ_y^2 behaves when calculated this way.

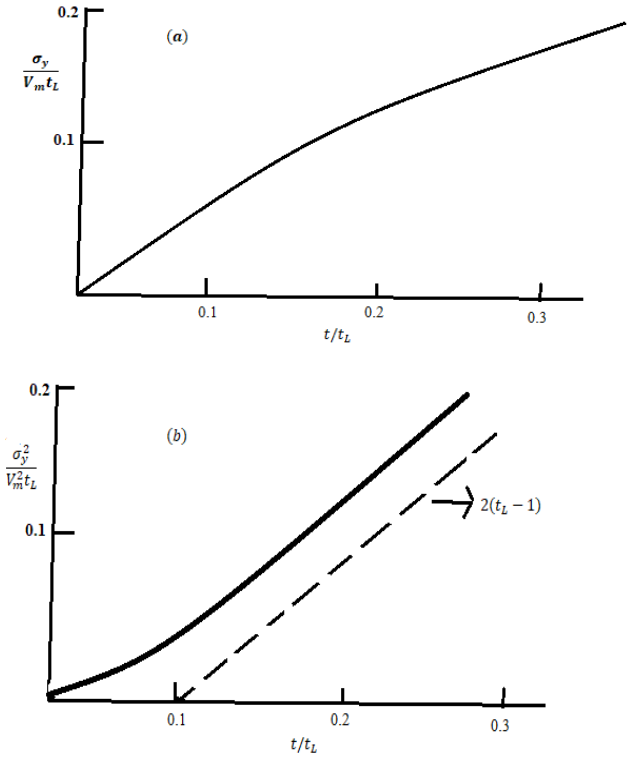

Fig. 2: shows how the standard deviation (σ_y) behaves on a linear and quadratic ordinate scale.

An alternate option the function provided in Eq. (3) and the Lagrangian correlation function have the same area under the $R(\tau)$ curve.

$$R(\tau) = exp\left\{-\frac{\pi}{4}\frac{\tau^2}{t_L^2}\right\} \quad (8)$$

The resulting dispersion is: This is an even function that satisfies the physical requirement at the origin that $R(\tau)$ should have a continuous tangent (implying finite accelerations).

© 2025 NSP
Natural Sciences Publishing Cor.

$$\sigma_y^2 = 2\overline{v^2}t_L\left[t\,erf\left(\frac{\sqrt{\pi}}{2}\frac{t}{t_L}\right)+\frac{2}{\pi}t_L exp\left(-\frac{\pi}{4}\frac{t^2}{t_L^2}\right)-\frac{2}{\pi}t_L\right] \quad (9)$$

with, $t_0 = t_L, t_1 = (2/\pi)t_L$, derived from Eqns. (5a) and (5b), the function in Eq. (9) produces a behavior that closely resembles that shown in Fig. (2). According to [30-31], when wave-like motions are present, R(τ) is positive. However, R(τ)accumulates strong negative loops, resulting in a considerably different behavior of diffusing clouds, including oscillations of cloud size.

Average Concentration Field of a Continuous Source

The fundamental theorem described the concentration field in a homogeneous field under the assumption that the entire distribution $P(x, y, z, t)$ is Gaussian (in the three spatial dimensions). The probability distribution of displacements at very short times $t \ll t_L$is proportional to the Gaussian distribution of turbulent velocity components, and the total displacement over a period greater than t_L may be regarded as independent. This occurs at diffusion times that are large in relation to the periods of order t_L at which the velocity is correlated for it. The average concentration field of an instantaneous point source can be found by assuming the dispersion in the sense that $\overline{xy} = \overline{yz} = \overline{xz}$ .The three mean square dispersions $\sigma_x^2 = \overline{x^2}$, $\sigma_y^2 = \overline{y^2}$, $\sigma_z^2 = \overline{z^2}$ then fully determine the distribution. The average concentration field of an instantaneous point source at a mean velocity U directed along the x-axis is as follows [32-33]:

$$\chi(x,y,z,t) = \frac{Q}{(2\pi)^{3/2}\sigma_x\sigma_y\sigma_z}exp\left\{-\frac{(x-Ut)^2}{2\sigma_x^2}-\frac{y^2}{2\sigma_y^2}-\frac{z^2}{2\sigma_z^2}\right\} \quad (10)$$

The standard deviations $\sigma_x, \sigma_y, \sigma_z$are therefore functions of time according to Equation (5). These are usually unequal in normal turbulent flow, and the mean square turbulent velocities usually differ even when the Lagrangian correlations are the same. The longitudinal (x) axis often disperses more quickly than the y and z axes. Turbulent movement-induced diffusion is a linear process, and composite fields of several sources can be defined by adding the fields of simple sources. In this instance, the superposition creates the composite field with a release rate of Q in g s^{-1} or its equivalent.

$$\chi(x,y,z) = \frac{Q}{(2\pi)^{3/2}}exp\left\{-\frac{(x-U\acute{t})^2}{2\sigma_x^2}-\frac{y^2}{2\sigma_y^2}-\frac{z^2}{2\sigma_z^2}\right\}\frac{d\acute{t}}{\sigma_x\sigma_y\sigma_z} \quad (11)$$

In order to perform the integration, it is essential to outline how the standard deviations σ_x, among others, relate to diffusion-time ť.. Equation (5a) indicates that the average cloud of the instantaneous-source ensemble increases linearly over time at short distances from the source.

$$\sigma_x = u_m t$$
$$\sigma_y = v_m t \quad (12)$$
$$\sigma_z = w_m t$$

where, u_m, v_m and w_m are turbulent velocities. For this simple dependence on time Eq. (11) may be integrated and yields:

$$\chi(x,y,z) = \frac{Qu_m}{(2\pi)^{3/2}v_m w_m r^2}exp\left(-\frac{U^2}{2u_m^2}\right)\left[1+\sqrt{\frac{\pi}{2}}\frac{Ux}{u_m r}exp\left(\frac{U^2x^2}{2u_m^2r^2}\right)erfc\left(-\frac{1}{\sqrt{2}}\frac{Ux}{u_m r}\right)\right] \quad (13)$$

where, we have written:

$$r^2 = x^2 + \frac{u_m^2}{v_m^2}y^2 + \frac{u_m^2}{w_m^2}z^2$$

When the relative turbulence intensity u_m/U is lower, the iso-concentration lines on the source's upstream side group together even more [34]. When this relative turbulence intensity is around 0.1, significant concentrations are frequently confined to a little cone downstream of the source. In narrow plumes like this, we have roughlyr ≅ x, so $U/u_m \gg 1$,.

$$erfc\left(-\frac{1}{\sqrt{2}}\frac{Ux}{u_m r}\right) \cong 2$$

After a few simple approximations, the second item in the brackets in Eq. (13) subsequently grows greatly in proportion to unity.

$$\chi(x,y,z) = \frac{q}{2\pi\sigma_y\sigma_z U}exp\left\{-\frac{y^2}{2\sigma_y^2}-\frac{z^2}{2\sigma_z^2}\right\} \quad (14)$$

The distribution is the same as cross sections of instantaneous point source clouds that have diffused over a period $t = x/U$ when the diffusion time $t = x/U$ is substituted back from Eq. (12). The material diffusing within each slice of the plume, dx long, is $q\,dt = q\,dx/U$. The slender-plume approximation is still valid a fortiori, but the approximation of Eq. (14) is adequate for practical purposes. Diffusion along y and z can be calculated with diffusion time $t = x/U$, which becomes comparable to the Lagrangian time-scale. The plume grows even more slowly than given by Eq. (12). By integrating the fields of instantaneous point sources, the average concentration fields of instantaneous or continuous (or those operating for a finite period) point, line, area, or volume sources can be estimated [35].

Evident Eddy Diffusivity

An eddy-diffusivity approach is the conventional method for parameterizing turbulent diffusion in the atmospheric boundary layer. It will be to differentiate between the concentration distributions realized in a particular trial $\bar{N}(x, t)$ and the ensemble-mean concentration field (χ) in the molecular diffusion equation such that

$$\chi(\mathbf{x}, t) = \bar{N}(\mathbf{x}, t) \quad (15)$$

The reasoning states that for a certain trial, the conservation of mass gives:

$$\partial N/\partial t = -\nabla.\boldsymbol{F} \quad (16)$$

If both molecular diffusion and bulk fluid motion contribute

© 2025 NSP
Natural Sciences Publishing Cor.

to the flux F:

$$\boldsymbol{F} = \boldsymbol{u}N - D\boldsymbol{\nabla}N \tag{17}$$

Because tracer concentration and fluid velocity are random variables in turbulent flow, they can be divided into "fluctuating" and "ensemble" mean components [15] as follows:

$$\boldsymbol{u} = \bar{\boldsymbol{u}} + \acute{\boldsymbol{u}}$$

$$N = \bar{N} + \acute{N} \tag{18}$$

Substitute from Eq. (18) in Eq. (17) on both sides of Eq. (16) (from Eq. (17)) yield the average flow as follows:.

$$\bar{\boldsymbol{F}} = \bar{\boldsymbol{u}}\chi + \acute{\boldsymbol{u}}\acute{N} - D\nabla\chi \tag{19}$$

Flux by turbulent movements is obtained by taking the average of Eq. (19), one gets as follows:

$$\overline{\boldsymbol{F}_t} = \overline{\acute{\boldsymbol{u}}\acute{N}} \tag{20}$$

Then, the average of Eq. (16) becomes:

$$\frac{\partial\chi}{\partial t} + \bar{\boldsymbol{u}}.\nabla\chi = -\boldsymbol{\nabla}.\bar{\boldsymbol{F}}_t + D\nabla^2\chi \tag{21}$$

By taking into account the point-source solution of Eq. (10), numerous additional solutions can be constructed using linear superposition. For this x-field, the left-hand side of Eq. (21) can be computed as follows [36]:

$$\frac{\partial\chi}{\partial t} + \bar{\boldsymbol{u}}.\nabla\chi = \frac{d\sigma_x}{dt}\left[\frac{(x-Ut)^2}{\sigma_x^3} - \frac{1}{\sigma_x}\right]\chi + \frac{d\sigma_y}{dt}\left[\frac{y^2}{\sigma_y^3} - \frac{1}{\sigma_y}\right]\chi + \frac{d\sigma_z}{dt}\left[\frac{z^2}{\sigma_z^3} - \frac{1}{\sigma_z}\right]\chi$$

$$= \sigma_x\frac{d\sigma_x}{dt}\frac{\partial^2\chi}{\partial x^2} + \sigma_y\frac{d\sigma_y}{dt}\frac{\partial^2\chi}{\partial y^2} + \sigma_z\frac{d\sigma_z}{dt}\frac{\partial^2\chi}{\partial z^2} \tag{22}$$

After ignoring the $D\nabla^2\chi$ term, the turbulent flux components can be identified as follows, which is consistent with Eq. (21).

$$F_{tx} = -\frac{1}{2}\frac{d\sigma_x^2}{dt}\frac{\partial\chi}{\partial x}$$

$$F_{ty} = -\frac{1}{2}\frac{d\sigma_y^2}{dt}\frac{\partial\chi}{\partial y} \tag{23}$$

$$F_{tx} = -\frac{1}{2}\frac{d\sigma_z^2}{dt}\frac{\partial\chi}{\partial z}$$

The differential equation is also solved by the point source solution given in Eq. (10):

$$\frac{\partial\chi}{\partial t} + U\frac{\partial\chi}{\partial x} = K_x\frac{\partial^2\chi}{\partial x^2} + K_y\frac{\partial^2\chi}{\partial y^2} + K_z\frac{\partial^2\chi}{\partial z^2} \tag{24}$$

And the following is the definition of "apparent eddy diffusivities":

$$K_x = \frac{1}{2}\frac{d\sigma_x^2}{dt}$$

$$K_y = \frac{1}{2}\frac{d\sigma_y^2}{dt} \tag{25}$$

$$K_z = \frac{1}{2}\frac{d\sigma_z^2}{dt}$$

It immediately follows from Taylor's theorem thatK_x, etc., depend on diffusion time.

$$K_x = \overline{\acute{u}^2}\int_0^t R(\tau)d\tau \tag{26}$$

Compared to molecular diffusion, turbulent dispersion happens far more quickly and in a qualitatively different way [37]. Two distinct "diffusivities" must be used to determine the field if two continuous sources are maintained concurrently in a turbulent field, one slightly upstream of the other. The existence of a straightforward linear relationship between mean flux and mean concentration gradient in the diffusion of an instantaneous point source, as in Eq. (23) if x, y, and z are major axes, and of course in all its linear super locations, is nevertheless of great practical value. A more adequate statistical model than that underlying the mixing-length argument should allow for a straightforward justification of the linear connections in Eq. (23) [38-40]. Eq. (14) provides an approximate description of a continuous point-source cloud.

$$U\frac{\partial\chi}{\partial x} = K_y\frac{\partial^2\chi}{\partial y^2} + K_z\frac{\partial^2\chi}{\partial z^2} \tag{27}$$

This corresponds to the narrow plume approximation used in its derivation and is a steady-state diffusion equation without diffusive flux in the x-direction. With the diffusion time $t = x/u$ substituted, the "diffusivities" K_y and K_z are once more defined as in Eq. (13):

$$K_y = \frac{U}{2}\frac{d\sigma_y^2}{dy} \tag{28}$$

Thus, observations of point-source cloud spreading can be used to determine the asymptotic behavior of this apparent eddy diffusivity as follows [41]:

$$K_y = \frac{v_m^2}{U}x \qquad (x \to 0)$$

$$K_y = v_m^2 t_L \qquad (x \to \infty) \tag{29}$$

The Lagrangian time scale t_L and the relative turbulence intensity v_m/U can also be calculated from observations of spreading clouds [14]. According to Taylor's theorem, the standard deviation of the dispersion parameters across the plume (σ_y or σ_z) grows linearly near the source ($\sigma_y/x = v_m/U$, $\sigma_z/x = w_m/U$), and at large distances it can be computed as follows. This means that the concentration distribution across a plume diameter is Gaussian.

$$\sigma_y^2 = 2\frac{v_m^2}{U^2}x_0(x - x_0) \tag{30}$$

Thus, x_0 is a sort of effective origin of the diffusion process, and $K_y = (v_m^2/U^2)x_0$ is the asymptotic eddy diffusivity. The exponential function $R = e^{-t/t_L}$ represents the Lagrangian correlation coefficient, which is calculated by applying Taylor's theorem in reverse (i.e., by double

© 2025 NSP
Natural Sciences Publishing Cor.

differentiating the $\sigma_y^2(x)$ curve).

The correlation coefficient's form also suggests $t_0 = t_1 = t_L$ (Eq. (5b)), which is represented by the double appearance of $x_0 = Ut_L$ in Equation (30). It is possible to successfully predict air diffusion using basic statistical theory and actual data, particularly the functional form of the standard deviations $\sigma_y(t)$ and $\sigma_z(t)$. However, the wind speed and air turbulence are not constant throughout the first 100 meters above the ground. Therefore, estimating the mean wind speed, which represents the real wind distribution in the homogenous field, is challenging. The length-scale of eddies, which is proportional to the height above ground level, is much more challenging. The mean concentration field above ground level caused by a continuous elevated point source of intensity $Q\,(gs^{-1})$ is properly described by the assumption that the ground is a perfect reflector, which is represented by a mirror-image source positioned below ground:

$$\chi(x,y,z) = \frac{Q}{2\pi U\sigma_y\sigma_z}\left[exp\left\{-\frac{y^2}{2\sigma_y^2} - \frac{(z-h)^2}{2\sigma_z^2}\right\} + exp\left\{-\frac{y^2}{2\sigma_y^2} - \frac{(z+h)^2}{2\sigma_z^2}\right\}\right] \quad (31)$$

where, the coordinate origin is vertically below the source at ground level and the source is situated at height h. Although determining the proper value of the "mean" wind speed U is challenging, defining the functions $\sigma_y(x)$ and $\sigma_z(x)$ is a significant challenge in and of itself, and the preceding formula is useful for predicting ground level concentrations:

$$\chi(x,y,z) = \frac{Q}{\pi U\sigma_y\sigma_z} exp\left\{-\frac{y^2}{2\sigma_y^2} - \frac{h^2}{2\sigma_z^2}\right\} \quad (31a)$$

At y = 0, one finds:

$$\chi(x,y,z) = \frac{q}{\pi U\sigma_y\sigma_z} exp\left\{-\frac{h^2}{2\sigma_z^2}\right\} \quad (31b)$$

When the exponential argument is -1 (i.e., $\sigma_z = h/\sqrt{2}$), the concentration reaches its maximum; however, over long distances, where $\sigma_z \gg h$, the concentration varies as $(\sigma_y\sigma_z)^{-1}$.Setting h=0 in the aforementioned formulae will yield the formula for the ground-level point source. Equation (31a) can also be used to calculate lines of constant mean concentration at ground level, which produce lengthy, cigar-shaped contours [42].

Initial Continuous Plume Phase:

For elevated sources, the dispersion parameters in a homogeneous field are predicted using Eq. (5a). An initial phase of diffusion can be characterized as follows when characterizing diffusion from ground-level sources near the ground, where the Lagrangian time scale becomes very short (very small eddies):

$$\sigma_y = i_y x$$
$$\sigma_z = i_z x \quad (32)$$

This is frequently true in the region of the ground where the highest concentrations at ground level are also noted. The structure and characteristics of atmospheric turbulence, including the height of measurement, ground roughness, and atmospheric stability, determine the turbulence intensities i_y, i_z. Under neutral stability conditions, turbulent velocities are roughly constant in the surface layer up to a height of 100 meters, after which they decrease with height. In contrast, the mean wind speed increases significantly (in the surface layer as the logarithm of the height), causing the relative turbulent intensity—which is the ratio of turbulent velocity to mean wind speed—to decrease with height. This means that the effective value of the turbulent intensity decreases with increasing source height and over rough ground turbulence as opposed to over a smoother surface [43]. The mean velocity distribution can be obtained using this connection for a neutral surface layer as follows:

$$U = \frac{u_*}{k} ln\frac{z}{z_0} \qquad for\ z \gg z_0, \qquad say\ z > 100z_0$$
$$\sqrt{\overline{\dot{v}^2}} = 2.2u_*$$
$$\sqrt{\overline{\dot{w}^2}} = 1.25u_* \quad (33)$$

where z_0 is roughness length, k is "Karman's constant," which is typically thought to be around 0.4, and u_* is friction velocity ($\sqrt{\tau_0/\rho}$, if τ_0 is shear stress at ground level, ρ air density. When Eqns. (32) and (33) are combined, the effective vertical turbulence intensities can be expressed as follows under neutral conditions:

$$i_y = \frac{0.88}{\ln z/z_0}$$
$$i_z = \frac{0.5}{\ln z/z_0} \quad (33a)$$

If the velocity distribution is logarithmic, the level $z = h/e$ is where the arithmetic average velocity between release height h and $z = z_0$ is reached. In a representation of diffusion using a homogeneous field model, it seems plausible to use the value of i_y, i_z appropriate to this level. Therefore, we determine the estimations for various release heights and surface roughness's under neutral conditions.

$$i_y = \frac{0.88}{\ln h/z_0 - 1}$$
$$i_z = \frac{0.5}{\ln h/z_0 - 1} \quad (33b)$$

Due to the turbulence intensity's dependency on the vertical heat flow, the relationship between the turbulent intensity and the different external parameters becomes highly complex in non-neutral situations. Significant fluctuations in the turbulent intensities i_y, i_z have been noted, ranging from relative intensities of more than 0.5 under high instability to negligible turbulence in prominent inversions (strong stability). Thus, as indicated in Table (1), six

© 2025 NSP
Natural Sciences Publishing Cor.

stability categories, numbered A through F, were created to address that [44-46].

Table 1: Pasquill stability categories

Surface wind	insolation			Night mainly	
Speed ms^{-1}	Strong	Moderate	Slight	overcast≥ 4/8 low wind	≤ 3/ 8 low wind
2	A	A-B	B	-	---
2-3	A-B	B	C	E	F
3-5	B	B-C	C	D	E
5-6	C	C-D	D	D	D
6	C	D	D	D	D

A -Extremely unstable, B -Moderately unstable, C -Slightly unstable D -Neutral, E -Slightly stable, F -Moderately stable.

Growth of Atmospheric Clouds Distinct from Concentrated Sources

The basic statistical theory anticipates an additional parameter, the Lagrangian time scale, at greater distances from the source, while the straightforward correlations of Eq. (32) only depend on relative turbulence intensity. Even while it is more difficult to determine a functional form of the standard deviations $\sigma_y(x), \sigma_z(x)$ using elementary theory, it is nevertheless a valuable tool in practice [47]. Power law formulations for the standard deviations can be suggested by analyzing experimental data on the expansion of clouds discharged at ground level:

$$2\sigma_y^2 = C_y^2 x^{2-n}$$
$$2\sigma_z^2 = C_z^2 x^{2-n} \quad (34)$$

where, the values of the variables n, C_y, and C_z depend on the source height and atmospheric stability. It was discovered that $n = 0.25$ under neutral conditions and that $C_y = 0.4\text{cm}^{1/8}$ and $C_z = 0.6\text{cm}^{1/8}$on flat grass land near ground level [29]. The Lagrangian correlation coefficient implied by Eq. (34) can be found by applying Taylor's theorem in reverse.

$$R(\tau) = \frac{(2-n)(1-n)C_y^2 U^{2-n}}{4\bar{v}^2}\tau^{-n} \quad (35)$$

$R(\tau) = \text{const.}\,\tau^{-n}$ exhibits a number of undesirable physical characteristics. For this form of $R(\tau)$, the integrals used to construct the time scales t_0 and t_L in Eq. (5b) diverge. This kind of correlation coefficient results in an implausible spectrum for a stationary stochastic process: at zero frequency, the spectral density becomes infinite. Such a mechanism seems to imply the existence of indefinitely huge eddies, yet it is difficult to give it any physical significance [48].

The Hay-Pasquill Technique for Predicting Cloud Spread

The relationship between Eulerian and Lagrangian statistics (autocorrelation functions, spectra, and, specifically, time scales T_E, T_L) is problematic. Because of the same turbulent field determines both Lagrangian and Eulerian "correlations" [49]. While the relevant values of $\acute{v}^2$and $\acute{w}^2$are found as Eulerian quantities as an average of $\overline{\acute{v}^2}$, $\overline{\acute{w}^2}$over the same sampling period s, σ_y and σ_z are calculated from concentrations averaged over a sampling time s. This equivalency took place at diffusion durations so brief that the particles maintained their initial turbulent velocities and the Lagrangian correlation coefficient remained unity. The fraction of the eddy spectrum that contributes to diffusion should be equal to that that contributes to the measured fixed-point mean square velocity when the sampling time is the same. The average Eulerian velocity during a suitably reduced period can be used to replicate a velocity record. For instance, if a particle is launched at time t_r along the y-axis, its simulated displacement over travel time t would be

$$y_T = \frac{t}{T}\int_{t_r}^{t_r+T} \acute{v}(\acute{t})\, d\acute{t} \quad (36)$$

where $\acute{v}(\acute{t})$ are Eulerian velocities, and the simulation time T is some fraction of the diffusion or travel time, for β is an empirical constant:

$$t = \beta T \quad (37)$$

In Eq. (36) the averaged Eulerian velocity ($1/T$ times the integral) multiplies the travel time. The relationship between Eulerian velocity and simulated displacement is almost identical with $x = \int_0^t u(\acute{t})d\acute{t}$ and the argument leading to Taylor's theorem applies, so that

$$y_T^2 = 2\acute{v}^2\beta^2 \int_0^T \int_0^t R_E(\tau)d\tau dt \quad (38)$$

where $R_E(\tau)$ is the Eulerian velocity autocorrelation, with $R_L(\tau)$ is the Lagrangian autocorrelation:

$$\sigma_y^2 = \overline{y^2}(t) = 2\bar{v}^2 \int_0^t \int_0^{\acute{t}} R_L(\tau)d\tau d\acute{t} \quad (39)$$

The two expressions are identical for all values of t if, in addition to Eq. (37), it is true that:

$$R_E(\tau) = R_L(\beta\tau) \quad (40)$$

or that the shapes of the Eulerian and Lagrangian correlations are identical after appropriate rescaling of the time axis. The prediction of diffusion is not very sensitive to the exact shape of the correlation coefficient and therefore the simulation technique based on Eulerian velocities gives in practice good diffusion predictions and the ensemble averages are replaced by time-averages over the chosen sampling time s, [50].

$$\bar{y}_T^2 \to \int_0^s y_T^2(t_r)dt_r \quad (41)$$

This procedure may be interpreted as forming a moving average velocity process:

$$\acute{v}_T(t_r) = \frac{1}{T}\int_{t_r}^{t_r+T} \acute{v}(\acute{t})\, d\acute{t} \quad (37a)$$

© 2025 NSP
Natural Sciences Publishing Cor.

The mean-square value over sampling time s gives the dispersion estimate

$$y^2(t) = t^2\overline{\acute{v}^2_{t/\beta,s}} \quad (38a)$$

where it bears repetition that $\overline{\acute{v}^2_{t/\beta,s}}$ is the mean-square value of the moving-average velocity process [51-52]. When the instrument used to determine lateral velocity fluctuations is a light directional vane, its output is azimuth angleθ, which is, for small angles very nearly

$$\theta = \frac{\acute{v}}{U} \quad (42)$$

A signal proportional to azimuth angle may be processed to form a moving average over period t/β, then squared and averaged over sampling time s to yield $\overline{\acute{\theta}^2_{t/\beta,s}}$The simulated mean-square displacement is then

$$y^2(t) = x^2\overline{\acute{\theta}^2_{t/\beta,s}} \quad (43)$$

where x = Ut is distance from the point of release. This may be written in a form identical with Eq. (32):

$$\sigma_y = i_y\big|_{t/\beta,s}x \quad (43a)$$

where $i_y\big|_{t/\beta,s} = \sqrt{\theta^2_{t/\beta,s}}$ is the effective value of lateral turbulent intensity for travel time t, sampling time s. An entirely analogous relationship holds for the vertical component:

$$\sigma_z = i_z|_{t/\beta,s}x \quad (43b)$$

Where i_z is evaluated from Eulerian record of the vertical velocity fluctuations$\acute{w}$. The Hay-Pasquill method gives good cloud-growth estimates in real-life atmospheric diffusion problems, when the character of atmospheric turbulence is far from ideal [53]. The appropriate value of the empirical constant $\beta = 4$ has given good results in many different situations. From an engineering point of view, in design estimates, a long series of Eulerian turbulence measurements may be utilized to establish diffusion climatology of a given site. Prior to building a chimney one could record turbulent velocities at e^{-1} times chimney height for a year or more and analyze the data to see with what frequency high or low values of σ_y, and σ_z would occur.

3. Results and Discussion

Concentration of I^{135} was obtained experimentally in convective layer at height 0.7 m, stack height 43 m with roughness length of 0.6cm [54]. Table (3) shows the meteorological data, the measured concentration of I135 isotope, the predicted concentrations by Gaussian using Eqns. (31) and (31a) below the plume centerlines. The predicted concentrations by Gaussian Brookhaven technique using the calculated dispersion parameters from Eq. (34) and Table (2) and the calculated effective height h=43+(12/u). Figs. (3& 4) explain the variation of measured and proposed concentration of I135 by Gaussian and Gaussian Brookhaven technique via horizontal distance in convective layer.

Table 2: Brookhaven National Laboratory dispersion parameterization scheme

Stability classes	Values of σ_y	Values of σ_z
A	$\sigma_y = 0.40x^{0.91}$	$\sigma_z = 0.41x^{0.91}$
B	$\sigma_y = 0.40x^{0.91}$	$\sigma_z = 0.41x^{0.91}$
C	$\sigma_y = 0.36x^{0.86}$	$\sigma_z = 0.33x^{0.86}$
D	$\sigma_y = 0.32x^{0.78}$	$\sigma_z = 0.22x^{0.78}$

Table 3: Comparison between the Gaussian, ground-level and observed crosswind- integrated normalized concentration at different downwind distance.

Run	Stability class	h (m)	Wind Direction (deg)	U_{10} m (m/s)	Q (Bq)	z(m)	Distance (m)	Observed Conc. (Bq/m^3	Gauss Model Eqns.(31,34) (Bq/m^3)	Gauss Brook. model (Bq/m^3)	Ground Gauss model Eqns.(31a,34) (Bq/m^3)	Ground Gauss Brook model (Bq/m^3)
1	A	600.85	301.1	4	1028571	5	100	0.032	0.018	0.024	0.032	0.012
2	A	801.13	278.7	4	1050000	10	98	0.038	0.073	0.043	0.015	0.038
3	B	973	190.2	6	42857.14	5	115	0.015	0.033	0.076	0.018	0.015
4	C	888	197.9	4	471428.6	5	135	0.197	0.074	0.144	0.092	0.160
5	A	921	181.5	4	492857.1	2	99	0.272	0.384	0.318	0.104	0.317
6	D	443	347.3	4	514285.7	8	184	0.188	0.224	0.186	0.149	0.252
7	C	1271	330.8	4	1007143	7.5	165	0.447	0.408	0.471	0.355	0.219
8	C	1842	187.6	4	1043571	7.5	134	0.123	0.104	0.103	0.174	0.175
9	A	1642	141.7	4	1033929	5	96	0.032	0.051	0.025	0.032	0.024

© 2025 NSP
Natural Sciences Publishing Cor.

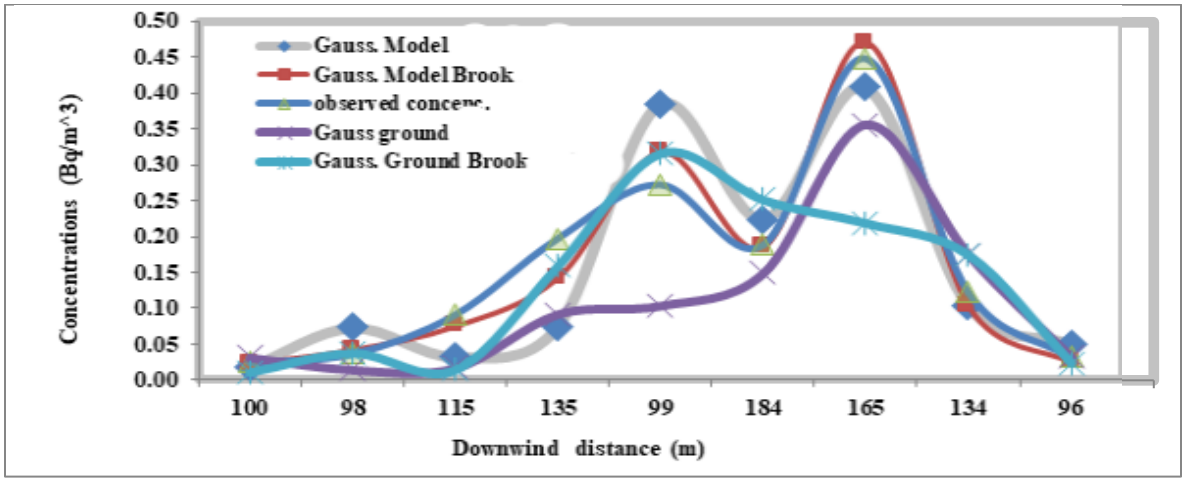

Fig. 3: The variations of observed and calculated concentrations (Bq/m3) by Gaussian plume models and Gaussian at ground via downwind distances (m).

Fig. (3) demonstrates that the Gaussian plume model and Gaussian concentrations at the ground using Eq. (34) using Brookhaven technique agree well and are closer to reported concentrations. Also, from this figure we find that the Gaussian plume model are better than the Gaussian at ground level with respect to observed concentrations of I^{135} (Bq/m^3) through the different values of the downwind distances (m).

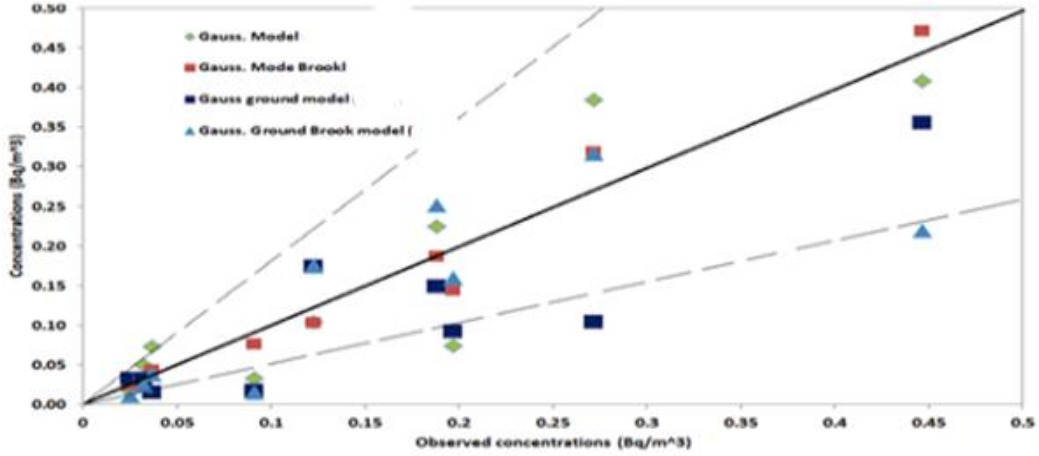

Fig. 4: Shows Gaussian, and the Gaussian at ground concentrations with observed concentrations (Bq/m3).

Fig. (4) Demonstrates that all predicted Gaussian model are inside a factor of two with respect to Observed concentrations of I135, but the most points of Gaussian at ground are inside a factor of two with respect the observed concentrations of I^{135}.

Statistical Evaluation

To describe the agreement between the predicted and observed concentrations statistical comparisons of the estimated dispersion parameters with the observed values were computed. The following statistical indicies were used as follows, NMSE is Normalized Mean Square Error, FB is Fraction Bias, COR is the Correlation coefficient and FAC2 Factor of Two (FAC2) [55-57].

1. Normalized mean square error (NMS): It is given by,

$$NMSE = \frac{(C_o - C_p)^2}{C_o C_p}$$

Where Co is the mean value of the observed concentration, Cp is the mean value the predicted concentration. Its value should be as small as possible for a good scheme.

2. Fraction BIAS: $FB = \frac{C_p - C_o}{}$

3. Correlation coefficient (R):

It describes the degree of association or agreement between the observed and predicted concentration:

$$\frac{(C_{oi} - C_o)(C_{pi} - C_p)}{\sigma_o \sigma_p}$$

Its value lies between 0 and 1 inclusive, R may assume any value between -1 and +1, if R=1 there is a perfect direct linear correlation between the observed and calculated concentrations, while R= -1 indicates perfect inverse linear correlation. If R=0 the two variables are not correlated.

© 2025 NSP
Natural Sciences Publishing Cor.

4. Fraction within a factor of two (FAC2):

It is defined as FAC2 = fraction of data for which $0.5 \leq C_p / C_o \leq 2$.

Table 4: Comparison between the predicted and observed concentrations in unstable conditions

Models	NMSE	FB	COR	FAC2
Gaussian model	0.16	0.03	0.90	0.97
Gaussian model (Brookhaven)	0.02	0.02	0.99	0.98

According to Table (4), the Gaussian using the Brookhaven technique and using Eq. (34) are inside of a factor of two with observed concentrations of I^{135}. The Gaussian concentrations using the Brookhaven method and Eq. (34) achieved 98% and 0.97%, of observed concentrations of I^{135} respectively.

Table 5: Comparison between the predicted and observed concentrations at ground level in unstable conditions

Models	NMSE	FB	COR	FAC2
Gaussian model using Eq. (34)	0.31	0.37	0.88	0.69
Gaussian model (Brookhaven)	0.07	0.15	0.77	0.86

According to Table (5) and Fig. (4), the observed concentrations of I^{135} are within a factor of two of the Gaussian concentrations at ground with the two techniques. The suggested Gaussian concentrations at ground are 86%, and 0.69% of the reported I^{135} concentrations, respectively. For all suggested Gaussian models, NMSE and FB are near zero.

4. Conclusions

In this work we introduce variables and statistical concepts applied to turbulence parameterization for estimating air pollutant concentration. The Gaussian plume model and Gaussian concentrations at the ground using Eq. (34) using Brookhaven technique agree well and are closer to reported concentrations. Also, we find that the Gaussian plume model are better than the Gaussian at ground level with respect to observed concentrations of I135 (Bq/m3) through the different values of the downwind distances (m). Also, all predicted Gaussian model are inside a factor of two with respect to Observed concentrations of I^{135} in unstable condition, but the most points of Gaussian at ground are inside a factor of two with respect the observed concentrations of I^{135}.The Gaussian using the Brookhaven technique and using Eq. (34) are inside of a factor of two with observed concentrations of I^{135}. The Gaussian concentrations using the Brookhaven method and Eq. (34) achieved 98% and 0.97%, of observed concentrations of I^{135} respectively. The suggested Gaussian concentrations at ground are 86%, and 0.69% of the reported I^{135} concentrations, respectively.

Acknowledgements

The authors thanks the Editor and the staff in the Journal of Ecology of Health & Environment (JEHE)

Author Contribution declaration in the manuscript.

Khaled S.M. Essa conceived the research idea and participated in writing the research and creating the illustrations.

Ahmed M. Mosallem writes the research and participated in creating the illustrations.

Fawzia Mubarak writing and participated in creating the illustrations

"Corresponding author": **Khaled S. M. Essa**

References

[1] B. D. Turner Workbook of atmospheric dispersion estimates: an introduction to dispersion modeling, Lewis Publishers, (1994).

[2] Y. T. Tritscher, R. Raz, Y. Levi, I. Levy, and D. M. Broday. Emissions vs. turbulence and atmospheric stability: A study of their relative importance in determining air pollutant concentrations, Science of the Total Environment, 733, doi: 10.1016/j.scitotenv.2020.139300, (2020).

[3] M. Coccia. The effects of atmospheric stability with low wind speed and of air pollution on the accelerated transmission dynamics of COVID-19", International Journal of Environmental Studies,78(1),1–27, (2021),, doi:10.1080/00207233.2020.1802937.

[4] M. Bourgoin. Some aspects of Lagrangian dynamics of turbulence. Mixing and dispersion in flows dominated by rotation and buoyancy. ffhal-02633932f (2018).

[5] P. E. Dimotakis. Turbulent mixing. Annual Review of Fluid Mechanics, 37, 329-356 (2005) doi:10.1146/annurev.fluid.36.050802.122015.

[6] Z. Hussain,M. Musalaiah, Venkata Ramachandra P, and Liyakhath Ahmed SK. A Review on Theoretical Air Pollutants Dispersion Models", International Journal of Pharmaceutical, Chemical and Biological Sciences, IJPCBS, 3(4), 1224–1230, (2013), www.ijpcbs.com.

[7] G. Balvet, Y. Roustan, and M. Ferrand. Derivation of model-consistent universal functions for second-order turbulence models and their implications on Lagrangian stochastic methods for thermally stratified atmospheric surface boundary layer flows. Phys. Rev. Fluids 10, 103801 (2025).

[8] H. J. S. Fernando, D. Zajic, Di Sabatino, S., Dimitrova, R., Hedquist, B., Dallman, A." :Flow, turbulence, and pollutant dispersion in urban

© 2025 NSP
Natural Sciences Publishing Cor.

atmosphere", Phys. Fluids 22, (2010).

[9] R. Stull. Practical Meteorology: An Algebra-Based Survey of Atmospheric Science. Version 1.02b. University of British Columbia, Vancouver, BC, Canada (2017).

[10] Namrata and N. D. Wagh. A Review on Atmospheric Dispersion System for Air Pollutants Integrated with GIS in Urban Environment", Nature Environment and Pollution Technology, 21(4):1553-1563 (2022).

[11] J. Pozorski and M. Wacławczyk. Mixing in turbulent flows: An overview of physics and modeling. MDPI AG. (2020), doi: 10.3390/pr8111379.

[12] S. Zilitinkevich, E. Kadantsev, I. Repina, E. Mortikov, and A. Glazunov. Order out of chaos: Shifting paradigm of convective turbulence. J Atmos Sci, 78(12), 3925–3932, (2021), doi:10.1175/JAS-D-21-0013.1.

[13] A. C. L. Chian, F. A. Borotto, T. Hada, R. A. Miranda, P. R. Muñoz, and E. L. Rempel. Nonlinear dynamics in space plasma turbulence: temporal stochastic chaos. Rev Mod Plasma Phys, 6(1), (2022), doi:10.1007/s41614-022-00095-z.

[14] N. Zolani. Turbulent diffusion and air pollution: A comprehensive review of mechanisms, impacts, and modeling approaches. World Journal of Advanced Research and Reviews, 23(03), 1511–1525, (2024).

[15] J. Sun, J. C. Nappo, L. Mahrt, Danijel Belušić, Branko Grisogono, David R. Stauffer, Manuel Pulido, Chantal Staquet, Qingfang Jiang, Annick Pouquet, Carlos Yagüe, Boris Galperin, Ronald B. Smith, John J. Finnigan, Shane D. Mayor, Gunilla Svensson, Andrey A. Grachev, William D. Neff. Review of wave-turbulence interactions in the stable atmospheric boundary layer. In Reviews of Geophysics, Blackwell Publishing Ltd, 956–993,(2015), doi: 10.1002/2015RG000487.

[16] R. A. Shaw. Particle-turbulence interactions in atmospheric clouds. Annu Rev Fluid Mech, 35, 183–227, (2003), doi: 10.1146/annurev.fluid.35.101101.161125.

[17] M. Schröder, T. Bätge, E. Bodenschatz, M. Wilczek, and G. Bagheri. Estimating the turbulent kinetic energy dissipation rate from one-dimensional velocity measurements in time. Atmos. Meas. Tech., 17, 627–657 (2024).

[18] L. Zhang, H. Zhang, Q. Li, X. Cai, and Y. Song. Vertical dispersion mechanism of long-range transported dust in Beijing: Effects of atmospheric turbulence. Atmos Res, 269, (2022), doi:10.1016/j.atmosres.

[19] B. Both, Z. Szánthó, R. Goda. The Problem of Turbulence Intensity Measurement in Comfort Ventilation. Int. Rev. Appl. Sci. Eng., 8 (1): 17–23, (2017), DOI: 10.1556/1848.2017.8.1.4.

[20] B. Papp, B. Ist´ok, M. Koren, M. Balcz´o, and G. Krist´of. Statistical assessment of the concentration fluctuations in street canyons via time-resolved wind tunnel experiments. Journal of Wind Engineering & Industrial Aerodynamics, 246 105665, (2024).

[21] X. Gao , X. Wang, and H. Shi. Multifractal Cascade Analysis on the Nature of Air Pollutants Concentration Time Series over China. Aerosol and Air Quality Research, 19: 2100–2114, (2019), doi:10.4209/aaqr.2018.10.0364.

[22] G. Tinarelli, L. Mortarini, S. Trini Castelli, G. Carlino, J. Moussafir, C. Olry, P. Armand, D. Anfossi. Review and validation of MicroSpray, a lagrangian particle model of turbulent dispersion. Geophysical Monograph Series, 200, 311–327, (2012), doi:10.1029/2012GM001242.

[23] J. W. Lu Bai, X. Ma ID and H. Lu. Air Pollution Forecasts An Overview. Int. J. Environ. Res. Public Health, 15, 780, (2018), doi:10.3390/ijerph15040780.

[24] T. Federico and B. Eberhard. Lagrangian Properties of Particles in Turbulence. Annual Review of Fluid Mechanics 41(1):375-404, (2009), DOI:10.1146/annurev.fluid.010908.165210.

[25] Y. R. Jung, W.G. Park, and O. H. Park. Pollution dispersion analysis using the puff model with numerical flow field data. Mech. Res. Commun., 30(4): 277-286, (2003), doi:10.1016/S0093-6413(03)00024-7.

[26] B. J. Tsuang. Quantification on the source/receptor relationship of primary pollutants and secondary aerosols by a Gaussian plume trajectory model: Part I theory. Atmos. Environ., 37(28): 3981-3991, (2003), https://doi. org/10.1016/S1352-2310(03)00471-0.

[27] M. Bourgoin and H. Xu. Focus on dynamics of particles in turbulence. New Journal of Physics, 16(8):085010, (2014).

[28] T. Abe, O. S. Takayuki & H. Taniai. Circular autocorrelation of stationary circular Markov processes. Stat Inference Stoch Process, 20:275–290, (2017), https://doi.org/10.1007/s11203-016-9154-0.

[29] G. T. Csanady, G. R. Hilst,, and N. E. Bowne. Atmos. Env. 2, 273, (1968),

[30] K. Adam, Janusz Urbański, Adam Kiczko, Marcin Krukowski, Piotr Siwicki. Turbulent intensity and scales of turbulence after hydraulic jump in rectangular channel. Ann. Warsaw Univ. Life Sci.– SGGW, Land Reclam, 48 (2): 99–109, (2016).

[31] R. Garimella. Characterization of Autocorrelation

© 2025 NSP
Natural Sciences Publishing Cor.

Function of Continuous Time Markov Chains", Report No: IIIT/TR/2016/-1, Centre for Communications, International Institute of Information Technology, Hyderabad 500 032, INDIA, (2016).

[32] A. Yerramilli, V.B.R. Dodla, and S. Yerramilli. Air pollution, modeling, and GIS-based decision support systems for air quality risk assessment. Eur. J. Oper. Res.,10(4): 220, (2011), DOI: 10.5772/22055.

[33] J. M. Leelossy. Dispersion modeling of air pollutants in the atmosphere: A review", Cent. Eur. J. Geosci., 6(3): 257-278, (2014), https://doi. org/10.2478/s13533-012-0188-6.

[34] LI. Shao-wu, W. Shu, W. Jian-ping, MI. Jian-chun. Effect of turbulence intensity on airfoil flow: numerical simulations and experimental measurements. Appl. Math. Mech. -Engl. Ed.,32(8), 1029–1038, (2011), DOI 10.1007/s10483-011-1478-8.

[35] A. Noormohammadi, W. Bing-Chen. Study of vertical line source dispersion in a turbulent channel flow. International Journal of Heat and Mass Transfer, 177, (2021).

[36] A. S. Pier, M. M. Pedro Soares, and T. João. A Combined Eddy-Diffusivity Mass-Flux Approach for the Convective Boundary Layer", Journal of the Atmospheric Sciences, Vol. 64, (2007).

[37] Benoit Cushman-Roisin. Beyond eddy diffusivity: an alternative model for turbulent dispersion. Environ Fluid Mech, (2008), DOI 10.1007/s10652-008-9082-7.

[38] R. Chris Rehmann1 and F. Timothy Duda. Diapycnal Diffusivity Inferred from Scalar Microstructure Measurements near the New England Shelf/Slope Front. Journal of Physical Oceanography, 30, (1999).

[39] J. W. Danielle and C. R. Rehmann. Eddy diffusivity near bubble plumes", Water Resources Research, 41, W09409, (2005), doi:10.1029/2004WR003896.

[40] L. Scott Stachelhaus and S. Bradley Moran. A simple differential diffusion model to account for the discrepancy between 223Ra- and 224Ra-based eddy diffusivities", Journal of Geophysical Research, 117, C03004, (2012), doi:10.1029/2011JC007500.

[41] K. S. M. Essa, M. Embaby. New formulations of eddy diffusivity for solution of diffusion equation in a convective boundary layer. Atmospheric Research, 85(1): 77-83, (2007).

[42] M. Fawzia. Estimation of Ground- level Airborne Concentration in an Urban Area. International Journal of Advanced Research, 1(7): 697-707, (2013).

[43] H. Peter. Modelling mean and turbulence fields in the dry convective boundary layer with the eddy-diffusivity/mass-flux approach", Boundary-Layer Meteorol.125:525–536, (2007), DOI 10.1007/s10546-007-9203-8.

[44] IAEA. Atmospheric Dispersion in Nuclear Power Plant Siting. S.S. No. 50-SG-S3, IAEA-Vienna, (1980).

[45] K. S. M Essa, M. Embaby; M. Fawzia and I. Kamel. Estimation of Seasonal Atmospheric Stability and Mixing Height by Using Different Schemes", International Journal of Advanced Research, 1(9):429-438, (2013).

[46] D. W. Jonathan Kahl, L. Hillary Chapman. Atmospheric stability characterization using the Pasquill method: A critical evaluation. Atmospheric Environment, 187:196-209, (2018).

[47] A.Daly and P. Zannetti. Air Pollution Modeling-An Overview. The Arab School for Science and Technology (ASST) (http://www.arabschool.org.sy) and The EnviroComp Institute, (2007), (http://www.envirocomp.org/).

[48] S. Bauer, M. S. Swenson, A. Griffa. Eddy mean flow decomposition and eddy diffusivity estimates in the tropical Pacific Ocean. Journal of Geophysical Research, 107(C10):3154, (2002), doi:10.1029/2000JC000613, 200.

[49] D. Anfossi, U. Rizza, C. Mangia, G. A. Degrazia, E. Pereira Marques Filho. Estimation of the ratio between the Lagrangian and Eulerian time scales in an atmospheric boundary layer generated by large eddy simulation", Atmospheric Environment, 40: 326–337, (2006).

[50] S. Friedrich, Q. Detlef. Lagrangian and Eulerian measurements of horizontal mixing in the Baltic", Tellus, 31(2):138 – 144, (2010), DOI:10.1111/j.2153-3490.1979.tb00890.

[51] J. D., E. Wilson, N. Ek Yee, and R. d'Amours. Lagrangian simulation of wind transport in the urban environment. Q. J. R. Meteorol. Soc., 135:1586–1602, (2009).

[52] J. D., E. Wilson, N. Ek Yee, and R. d'Amours. Erratum to Lagrangian simulation of wind transport in the urban environment. Q. J. R. Meteorol. Soc., 136, 552, (2010).

[53] S. D. Anna, Kerstin Stebel, Massimo Cassiani, Hamidreza Ardeshiri, Arve Kylling, Soon-Young Park, Ignacio Pisso, Norbert Schmidbauer, Jan Wasseng, and Andreas Stohl. Observations of artificially released SO_2 puffs using a tomographic setup of six UV cameras", Atmos. Meas. Tech., 20:7571, (2018).

© 2025 NSP
Natural Sciences Publishing Cor.

[54] M. Fawzia. Atmospheric dispersion modeling and application to radioactive releases from Nuclear Reactors. Faculty of girls for arts, science and education, Ain Shams University. 2004. Ph.D.

[55] H. Leonardo, F. Davide, L. Henrique de Melo. Comparison of plume lateral dispersion coefficients schemes: Effect of averaging time", Atmospheric Pollution Research, 7:134-141,(2016).

[56] K. S. M. Essa, N. M.Aziz, S. H. Hany, M. Fawzia and A. K. Ayman. Studying the variation of eddy diffusivity on the behavior of advection diffusion Equation", NRIAG Journal of Astronomy and Geophysics 7:10–14, (2018).

[57] K. S. M. Essa, N. M. Aziz, S. H. Hany, M. Fawzia, A. M. Mosallem and A. K. Ayman. Dispersion from Two Dimensions Time-Dependent and Three Dimensions of Diffusion Equation in Different Stability Conditions. Interciencia Journal 44(4), (2019).

© 2025 NSP
Natural Sciences Publishing Cor.